



High-throughput imaging surface plasmon resonance biosensing based on ultrafast two-point spectral-dip tracking scheme

YOUJUN ZENG,¹ XUELIANG WANG,¹ JIE ZHOU,¹ RUIBIAO MIYAN,¹
JUNLE QU,¹ HO-PUI HO,² KAIMING ZHOU,³ BRUCE ZHI GAO,⁴
JIAJIE CHEN,^{1,5}  AND YONGHONG SHAO^{1,6}

¹College of Physics and Optoelectronics Engineering, Key Laboratory of Optoelectronic Devices and Systems of Ministry of Education and Guangdong Province, Shenzhen University, Shenzhen 518060, China

²Department of Biomedical Engineering, The Chinese University of Hong Kong, Shatin, Hong Kong 999077, China

³Aston Institute of Photonic Technologies, Aston University, Birmingham B4 7ET, UK

⁴Department of Bioengineering and COMSET, Clemson University, Clemson, SC 29634, USA

⁵cjj@szu.edu.cn

⁶shaoyh@szu.edu.cn

Abstract: Wavelength interrogation surface plasmon resonance imaging (λ SPRi) has potential in detecting 2-dimensional (2D) sensor array sites, but the resonance wavelength imaging rate limits the application of detecting biomolecular binding process in real time. In this paper, we have successfully demonstrated an ultrafast λ SPRi biosensor system. The key feature is a two-point tracking algorithm that drives the liquid crystal tunable filter (LCTF) to achieve fast-tracking of the resonance wavelength movement caused by the binding of target molecules with the probe molecules on the sensing surface. The resonance wavelength measurement time is within 0.25s. To date, this is the fastest speed ever reported in λ SPRi. Experiment results show that the sensitivity and dynamic are 2.4×10^{-6} RIU and 4.6×10^{-2} RIU, respectively. In addition, we have also demonstrated that the system has the capability of performing fast high-throughput detection of biomolecular interactions, which confirms that this fast real-time detecting approach is most suitable for high-throughput and label-free biosensing applications.

© 2020 Optical Society of America under the terms of the [OSA Open Access Publishing Agreement](#)

1. Introduction

Surface plasmon resonance (SPR) biosensors with the capability of label-free, real-time and high sensitivity, has been an important tool for exploring intermolecular interactions, and widely used in the biological field [1–4]. With the rising demand for biotechnology development, simultaneous detection of multiple samples is imperative, and the high-throughput is also an important direction in the future development of biology. The combination of imaging with SPR technology has enabled high-throughput biosensing on 2D array and monitoring various biomolecular interactions in parallel [5–7].

So far, there are mainly four interrogation modes for the SPR sensing technology, including interrogation mode of intensity, angle, wavelength, and phase. When conducting high-throughput imaging detection, the dynamic detection range is an important parameter of the SPRi sensors since the refractive index of samples on detection sites differs from each other. Normally, the dynamic range of intensity and phase interrogation sensors are 10^{-3} and 10^{-4} RIU, respectively [8]. The narrow dynamic range limits the application of SPRi sensors. Comparing to intensity and phase interrogation sensors, wavelength and angle interrogation sensors can provide larger dynamic range (10^{-2} RIU) [9]. Angle interrogation SPR sensors generally exploit a laser as the excitation source, while the laser speckle would decrease the imaging quality. In addition, the

different incident angle also introduces image distortion because of the coupling prism. However, under the wavelength interrogation mode, one can flexibly select optimal excitation wavelengths for different samples [10]. And the wavelength interrogation mode has good uniformity for different sensing sites of samples. Therefore, wavelength interrogation is considered to be an optimal SPR technology for imaging detection.

Yuk et al. first proposed the λ SPRi sensor which employed the spectral point-by-point scanning on sensor chip. By analyzing the reflected light spectra, the resonance wavelength of each detection site is obtained. The system achieved the detection of the process of protein array interaction. The duration of imaging one circular sample site with a diameter of 2 mm is 180 s [11]. Liu Le et al. also proposed a λ SPRi sensor scheme, in which a grating is adopted to scan the 2D sensor chip line by line to obtain the spectrum of reflected light. Their results show that imaging a region of $8 \times 8 \text{ mm}^2$ takes about 60 s [12]. Although those point-scanning or line-scanning technologies can image a whole 2D sensor chip and achieve high-throughput detection, the imaging speed does not satisfy the requirement of real-time monitoring of biomolecular binding process.

By utilizing 2D detector, one can directly get the images from the sensor, which free from point or line scanning, thus enables rapid imaging. The 2D detector combining with incidence wavelength scanning is also a possible way to achieve λ SPRi sensor with fast detection performance [13]. However, because of the existence of the wavelength scanning device's responding time, the total detection time will increase with the number of wavelength scanning points. Additionally, in order to prevent the resonance wavelength from exceeding the wavelength scanning range when the sample's refractive index is changing, the scanning range usually initially set to a wider one so the number of wavelengths scanning points also inherently increased. Thus, for the above reasons, the detection speed has been greatly limited in traditional λ SPRi devices. To increase the imaging speed, Sereda et al. proposed the 5-points fitting algorithm which can reduce the number of scanning points in each cycle, and utilized a monochromator to scan the incidence wavelength and a CCD is implemented as the imaging sensor, the imaging time is about 10 s [14]. In our previous studies, we also proposed several wavelength interrogation methods with high imaging speed. We have developed a feedback loop technique, in which the spectral scanning range can be dynamically adjusted in accordance with the position of resonance wavelength [15]. Our system used the liquid crystal tunable filter (LCTF) to track fast SPR dip movement induced by the binding of target molecules to the sensor surface. The imaging time of system has reduced to 0.7 s [16]. Moreover, the implementation of the LCTF has enabled rapidly wavelength scanning without any mechanical movement. Based on the feedback loop method, the system has been optimized further, we used an acousto-optic tunable filter (AOTF) to scan the incidence wavelength and a white light laser to excite SPR phenomenon, the imaging time of system was further reduced to 0.33 s [17].

In this paper, we propose a novel λ SPRi biosensor based on a two-point tracking algorithm. The system uses the LCTF to flexibly scan the incidence wavelengths, and a CMOS is employed to obtain the SPR images from the 2D sensing surface. Moreover, the two-point tracking algorithm has greatly reduced the number of scanning points to two in each scanning cycle. And we have achieved an overall image measurement time of 0.25 s, which is the shortest time that one can achieve nowadays on λ SPRi sensors.

2. Experimental setup

Figure 1 shows the schematic of our experimental setup based on the two-point tracking algorithm. The 100 W halogen tungsten lamp is the excitation light source, a bandpass filter selects a wavelength window with a center of 610 nm and full width half maximum (FWHM) of 220 nm. Light from the lamp is coupled into the multimode optical fiber, and the light is collimated by lens group. The LCTF (VariSpec, VIS-10-20-STD) is the wavelength scanning device, the

filtered narrow-band light's FWHM is 10 nm, the spectral resolution and the response time are 0.5 nm and 25 ms respectively. The LCTF manipulates the light into a narrow-band parallel light that goes to the sensing unit. The sensing unit is based on Kretschmann configuration which is composed of a prism, a sensor chip and flow chambers. The prism is made by BK7 glass (refractive index: 1.515 RIU), the sensor chip is composed of a glass slide coated with a 48 ± 2 nm thick gold film, and a chamber is fabricated for sample injection and measurement. In addition, noted that the optimal incidence angle is different for different samples, in order to find the most suitable incidence angle, in the experimental initialization, we first estimated the best incident wavelength using Fresnel equations and the equation for the reflectivity of the single-layer membrane [18–20]. Subsequently, based on this best incident wavelength, we manually adjusted the incidence angle to achieve minimum average intensity and fixed this optimal angle. Therefore, the optimal incident angle that can accommodate all the sensing sites in the whole 2D detection region is obtained. In the sensing unit, the incident light is coupled by a prism to excite SPR phenomenon on the surface of sensor chip. The reflected light passed the imaging lens group, and the intensity value of each position on the sensor chip is captured in parallel by a CMOS (The image source, 33UX252). The control software of our system is by a home-made Labview program. When system is working, the CMOS takes the image of the sensor chip after the LCTF switches the incidence wavelength. Each pixel on the image of sensor chip serves as an independent detecting site. When one wavelength scanning cycle is completed, by analyzing the series of images, one can acquire the SPR spectral curve, and get the resonance wavelengths of different detecting sites.

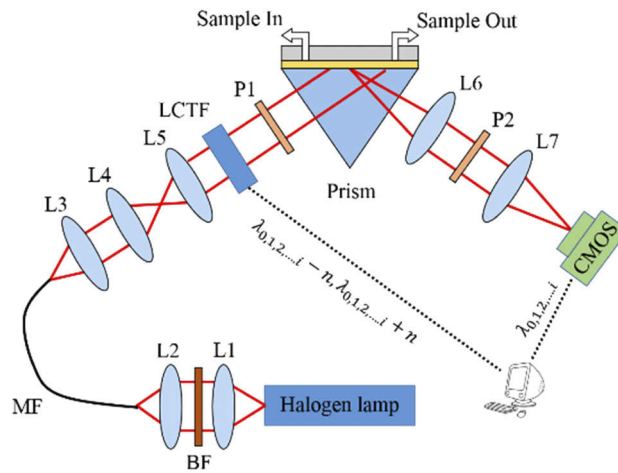


Fig. 1. Schematic of our two-point tracking SPRi system in the Kretschmann configuration. L1-L7, lens; BF, band filter; MF, multimode fiber; DA, diaphragm aperture; LCTF, liquid crystal tunable filter; P1 and P2, polarizers.

3. Two-point tracking algorithm

Figure 2 illustrates the operation principles of our system. In the 1st round scanning, when sample refractive index is n_0 , the LCTF scans the wavelengths in small steps at a larger spectral range of about 100 nm (dotted red curve), then we calculate the baseline resonance wavelength λ_0 via 7th-order curve fitting. Based on this fitting curve, in the vicinity of λ_0 , we extract a narrower local spectral region from $\lambda_0 - \Delta\lambda$ to $\lambda_0 + \Delta\lambda$, and the $\Delta\lambda$ is a constant to specify the spectral range which meets $\Delta\lambda \leq 10$ nm (The detail of $\Delta\lambda$ will be discussed in the following section). Then we fit this local spectral region via 2nd-order curve fitting and obtain its expression as

formula 3.1, and noted that the 2nd-order coefficients a is then reserved for all the subsequent calculations. In the second-round scanning, If the refractive index is changed, for example, from n_0 to n_1 , with the pre-known 2nd-order coefficients a , the substitution of the intensity results of I_{-n_1}, I_{+n_1} at the two wavelengths of $\lambda_0 - \Delta\lambda, \lambda_0 + \Delta\lambda$ into formula 3.1 will produce an updated coefficient b , and then a different dip wavelength of λ_1 (In Fig. 2, the red dotted curve transforms into a red solid curve with $2\Delta\lambda$ width) is calculated using formula 3.2.

$$I = a\lambda^2 + b\lambda + c \quad (3.1)$$

$$\lambda_i = \frac{b}{2a} \quad (3.2)$$

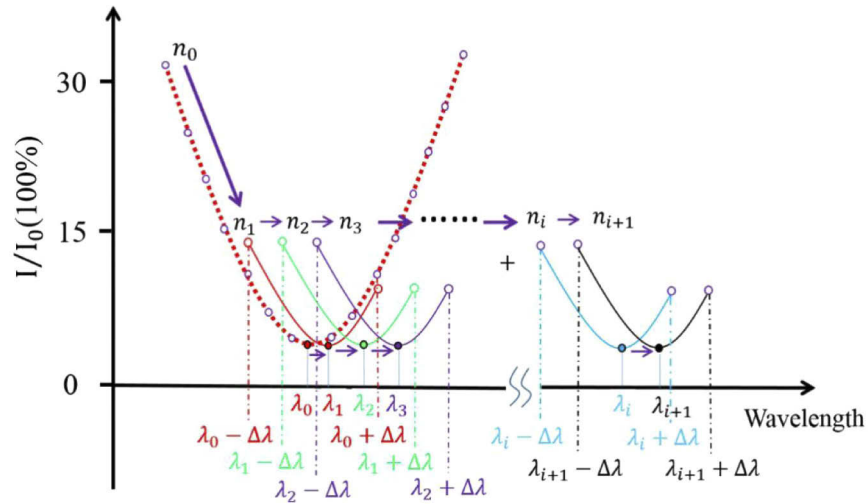


Fig. 2. Schematic showing the two-point tracking algorithm. n_0, n_1, \dots, n_i and n_{i+1} represent a series of dynamic samples' refractive index values. The red dashed represent SPR curve obtained by initial larger wavelength range scanning; other solid lines are the partial SPR plots near their SPR dips under the different refractive index values which derived from two-point tracking algorithm.

While if the refractive index n_0 remains constant, the same procedure will produce an identical dip wavelength of λ_0 . Moreover, the translation of dip wavelength also triggers two new scan wavelengths, which are $\lambda_1 - \Delta\lambda$ and $\lambda_1 + \Delta\lambda$, and they are preserved for the next period wavelength scanning. Subsequently, if refractive index continues to change from n_1 to n_2 . The same process will continue to run until the system has identified the next new resonance wavelength λ_2 , after which the next scanning wavelengths are triggered and modified to $\lambda_2 - \Delta\lambda, \lambda_2 + \Delta\lambda$, then the following new loops start. In summary, as shown in Fig. 2, in every scanning cycle, we only need to conduct two-point wavelengths scanning, the refractive index n_{i+1} in each cycle will produce two updated scan wavelengths of $\lambda_{i+1} - \Delta\lambda$ and $\lambda_{i+1} + \Delta\lambda$. And λ_{i+1} is generated by the wavelengths of $\lambda_i - \Delta\lambda$ and $\lambda_i + \Delta\lambda$ in previous scanning cycle.

Moreover, we also analyze the accuracy and the feasibility of this two-point scanning method. Noted that if the number of data points which used to fitting is less than the order of curve, there will be deviation between the fitting curve and the actual SPR curve, and a wider spectrum range will require a larger fitting order [14]. In our experiment, we used the 2nd order fitting. To analyze the deviation between actual and fitting SPR curve and find an optimal scanning spectrum range ($2\Delta\lambda$), we simulated it in different spectral width under 2nd order fitting. First, we generate an ideal SPR spectral curve governed by Fresnel formula [17,18], and obtain its

resonance wavelength λ . Then we extracted a series of spectra from this ideal SPR spectral curve which possess the same resonance wavelength λ while with different spectrum width ranging from 1 nm to 100 nm. Subsequently, we applied the 2nd order fitting on those series of spectra and summarize the deviation between actual resonance wavelength λ and resonance wavelength obtained from their 2nd order fitting curve. As the results in Fig. 3 indicate, with the increment of spectrum width, the deviation increases dramatically, and when the width of spectrum reduces to a certain value, the deviation is trivial. It shows that when the spectrum width is less than 20 nm, the deviation reduces to about 0.01 nm, and that is our system's resonance wavelength detection resolution. Therefore, after acquisition of the resonance wavelength λ , we can calculate the next moment resonance wavelength λ' by any two points in the range from $\lambda - \Delta\lambda$ to $\lambda + \Delta\lambda$ ($\Delta\lambda \leq 10$ nm) with high accuracy. On the other hand, considering that the intensity is weaker near the resonance wavelength where more random noise is interfering, we choose the scanning wavelengths at two extremes, i.e. $\lambda - 10$ nm and $\lambda + 10$ nm where the corresponding light intensities are relatively larger, so the SNR (signal to noise ratio) can be improved.

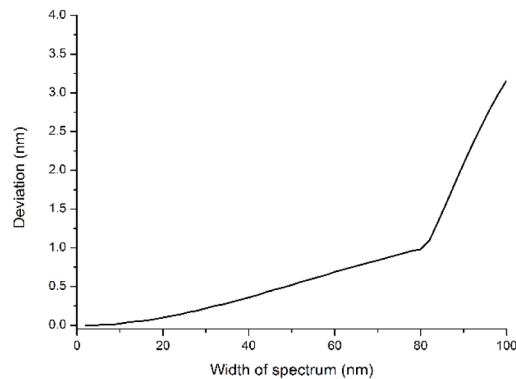


Fig. 3. The deviation between the calculated resonance wavelength and the real value under different spectral scanning widths in second-order fitting.

For 2D sensor array, different sensor sites can manifest different resonance wavelengths, the scan wavelengths should cover all the possible resonance positions in all the sensor sites. After complete initial large range wavelength scanning, a series of resonance wavelengths in different sensing site are obtained $\lambda_1, \lambda_2, \lambda_3, \dots, \lambda_k$. To have appropriate scan parameters to accommodate different sites' situation, the scan wavelengths are initially set to $\bar{\lambda} - \Delta\lambda$ and $\bar{\lambda} + \Delta\lambda$, where $\bar{\lambda} = \frac{\lambda_1 + \lambda_2 + \lambda_3 + \dots + \lambda_k}{k}$. First, based on the relationship between resonance wavelength and refractive index, the change of resonance wavelength of 20 nm is corresponding to a refractive index change ($2\Delta n_{20nm}$) of 1.2×10^{-2} RIU. Therefore, if the refractive index variation range of different sites is within the range of Δn_{20nm} , the system can get λ SPRi for all sample's detecting sites by scanning at two wavelengths at $\Delta\lambda = 10$ nm. For example, if the largest variation of resonance wavelength of each site is 6 nm, then our λ SPRi system can detect all the sites of one sample using two-point scanning. However, if the largest refractive index variation Δn from each site is larger than δn_{20nm} , the induced resonance wavelength translation will exceed 10 nm in next moment. In this situation, the adoption of 2nd order curve fitting becomes inaccurate for the resonance wavelength calculation. To address this issue, our system will automatically add one or more supplementary wavelength scanning points to conduct a cycle of re-scanning, and for each additional scanning wavelength, the covered bandwidth will increase by a step of 10 nm, and the number of additional scanning wavelengths will increase until the all resonance wavelengths from whole sensing sites can be calculated.

4. Results and discussions

The dynamic range is an important parameter that describe the range of detection. To assess our λ SPRi sensor, we tested it using a series of saline water with concentrations ranging from 0% to 20% in increments of 5% by volume, corresponding to a refractive index range from 1.3330 to 1.3885 RIU. During the testing, the incident angle was fixed to 72.5° which is the optimal SPR incident angle for water [5]. The 3×3 array sensor sites were divided evenly on the sensor surface, and these nine sites were detected simultaneously. As the results in Fig. 4 show, the resonance wavelength variation and the refractive index have a positive linear relation.

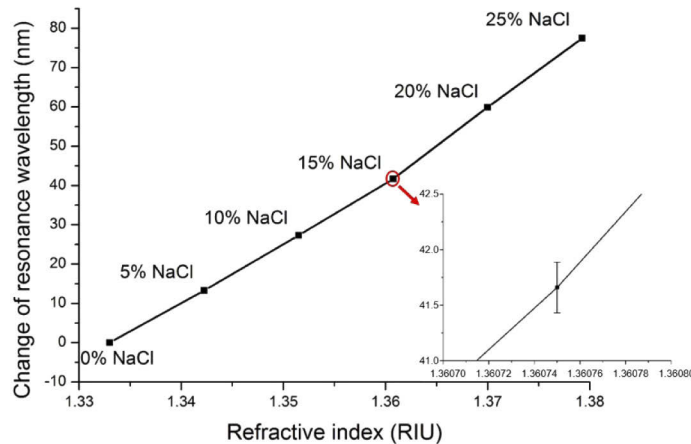


Fig. 4. Resonance wavelength shifting versus saline water concentration on 3×3 array on the SPR chip. Noted that each data point in the figure is the average value of nine detection sites. The inset is the zoom-in figure at the 15% saline water concentration.

Another importance technological parameter for a sensing system is the sensitivity which can be calculated from formula 4.1 [21], where σ_{RI} is sensitivity, the δn is the refractive index change, the $\delta \lambda$ is the corresponding shift of resonance wavelength, and the σ_{SD} is the root mean square (RMS) noise of our system.

$$\sigma_{RI} = \frac{\delta n}{\delta \lambda} \Delta \sigma_{SD} \quad (4.1)$$

To access the sensitivity, we detected the shift of the resonance wavelength induced by small variation of saline water concentration. And the results are illustrated in the Fig. 5(a). Then, because the signal intensity is relatively weaker near the resonance wavelength, we conducted multiple imaging and obtain the averaged value to reduce the random noise. As shown in Fig. 5(b), the RMS noise is reduced with the increasing of averaging time, after the number of averaging exceed 15, RMS noise tend to become stable and small. In our experiments, to ensure best performance, the number of averaging is set to 20, so it totally costs $2 \times (25\text{ms} + 5\text{ms} \times 20) = 250\text{ms}$ for two wavelengths scanning, where 25 ms is the response time of LCTF and 5 ms is the exposure time of CMOS. Therefore, based on the aforementioned calculation and analysis, the sensitivity of the system is 2.4×10^{-6} RIU.

In addition, we also conducted traditional large range uniform-step scanning mode [14] to verify the accuracy of the two-point tracking algorithm. In traditional scanning mode, the step and spectrum width are 1 nm and 100 nm respectively, and the order of generalized polynomial fitting is 7th order. We detected difference concentrations of saline using two different scanning modes under the same experimental condition. And results are illustrated in Fig. 6 it indicates that the two-point scanning mode measurement method is coincided with the traditional large

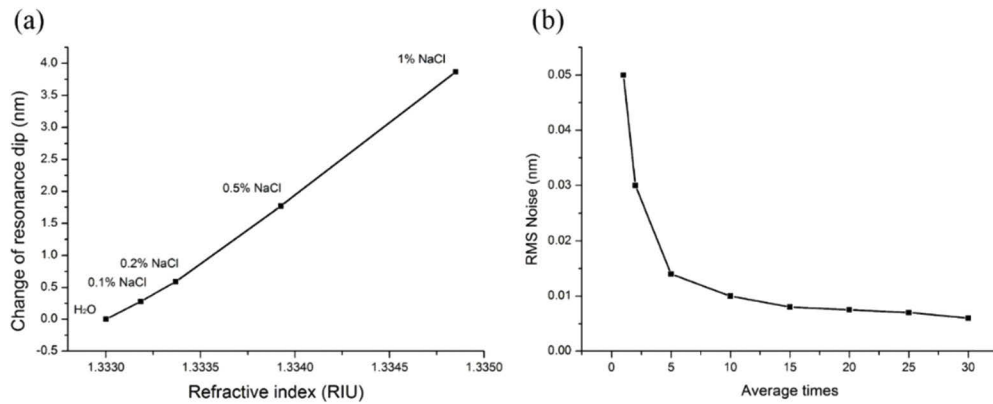


Fig. 5. The sensitivity test results. (a) The resonance wavelength shift obtained from low concentration saline water. (b) The relation between number of averaging and RMS noise.

range uniform-step scanning mode. Therefore, the accuracy of two-point tracking algorithm is comparable to the traditional whole spectral range scanning method.

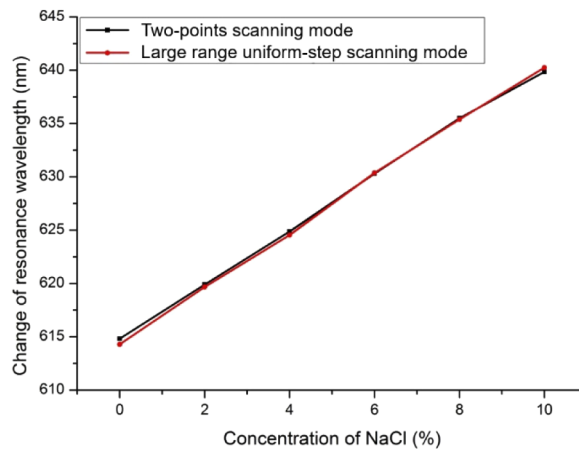


Fig. 6. Resonance wavelength obtained from saline water concentration variation (from 0% to 25%) via two-point scanning mode and traditional large range uniform-step scanning mode.

Moreover, we also tested the capability of our λ SPRi sensor for monitoring biomolecular interactions, we performed real-time monitoring of binding interactions between protein A and human IgG antibody (Solarbio, Shanghai, China). In the experiment, the sensor chip was first rinsed by deionized water, and dried with nitrogen gas, then placed onto the prism, the chip was attached to the coupling prism via a drop of refractive index matching oil. A three-channel flow chamber was adopted for injecting sample. And the probe fixation process is: 1) Phosphate buffered saline (PBS, 0.01 M, pH = 7.4) was injected into the 3 channels respectively and flushing for 5 min, and then the resonance wavelength of three channels is monitored in real time; 2) When the resonance wavelength was stable, probe A (100 μ g/ml) was injected into the three channels simultaneously in a flow rate of 30 μ l/min, when the protein A were steadily bonded on the sensing surface, resonance wavelengths become stable, then PBS was injected.

In the biological binding process, the three channels were injected with PBS, human IgG in concentration of 2 mg/ml and 1 mg/ml respectively, the channel with PBS is reference channel,

the other two channels are reaction channels. Before the chemical binding, the system conducted wavelength scanning of the sensing surface and stored the imaging data. The corresponding resonance wavelengths were recorded for all channels. When the resonance wavelengths reached stationary status, PBS were injected to wash the nonspecific binding sites. After obtaining steady baseline, the system imaged the sensor chip again.

As shown in Fig. 7(a), we obtained the time responsive curve of resonance wavelength change upon biological sample injection in three channels. The black curve is the reference channel, the red and blue curve are the reaction channels. The real-time wavelength detection diagram of the reference channel is unchanged before and after the reaction, while the resonance wavelength in the reaction channel is significantly different after the reaction, which is induced by the specific binding of antigen and antibody. Moreover, the 2D λ SPRi scheme also allows us to obtain the 2D resonance wavelength difference in each pixel before and after the reaction of the sensing surface. As illustrated in Fig. 7(b), the color of each pixel in the figure represents the resonance wavelength shift on the sensing surface before and after the reaction. Therefore, this fast 2D λ SPRi scheme is also favorable for real-time 2D bio-reaction monitoring.

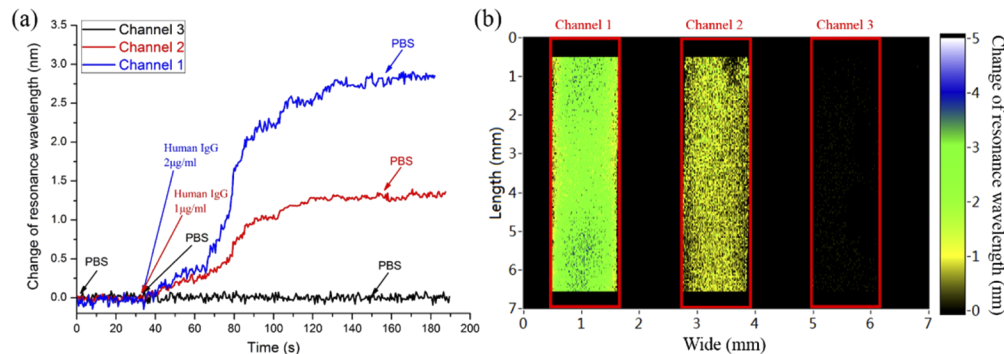


Fig. 7. Measurement of antigen-antibody interaction between probe A and human IgG. (a) Real-time wavelength response of three channels. The arrow indicated the very moment that the corresponding bio-samples are injected (b) The image of shift resonance wavelength, the samples introduced in the three channels from left to right are 2 mg/ml, 1 mg/ml human IgG and PBS.

5. Conclusions

Herein, we have demonstrated a novel fast λ SPRi sensor based on two-point tracking algorithm, and the scheme is free from mechanical moving parts. The combination of LCTF for incident light wavelength scanning and CMOS for 2D imaging has made our system capable of detecting multiple samples simultaneously and rapidly. In addition, the two-point tracking algorithm has reduced the number of scanning points per cycle to two. It has greatly mitigated the time consumption for wavelengths selection in scanning device. Compare to a conventional λ SPRi system, our device shows high sensitivity and large dynamic range. And the speed of imaging is among the fastest reported in the literature [5,22–23]. Our experiments have shown that the system sensitivity and the dynamic range are 2.4×10^{-6} RIU and 4.6×10^{-2} RIU respectively, and the imaging speed is 0.25 s per frame. The antigen-antibody interaction results also verified the biosensing capability for simultaneous detection in multiple sites. Therefore, the reported scheme is a powerful tool for monitoring multi-sample biomolecular interactions in real time.

In terms of future optimization, noted that there is a sensitivity disparity between the theory and our system which is induced by the spectral bandwidth (10 nm) from the wavelength switching device LCTF. If one chooses a high-performance filter as the wavelength switching device which

can provide a narrower bandwidth, the sensitivity can be further improved. As for the dynamic range, it is also limited by the excitation spectrum range of lamp. If the light source with larger spectrum range is adopted, the dynamic range can be further expanded. In addition, the speed of detection can also be further raised by using AOTF (acousto-optic tunable filter) whose wavelength switching time is only 2~4 ms. Moreover, the sensor's exposure time is another reason that limit the speed of detection. The speed can be further increased if one can improve the efficiency of light utilization.

Funding

National Key Research and Development Program of China (2017YFB0403804); Science, Technology and Innovation Commission of Shenzhen Municipality (CYJ20180305124754860, JCYJ20180228162956597); Guangdong Science and Technology Department (2017B020210006, 2018A030310544); National Natural Science Foundation of China (61527827, 61775148).

Disclosures

The authors declare no conflicts of interest.

References

1. B. Liedberg, I. Lundström, and E. Stenberg, "Principles of biosensing with an extended coupling matrix and surface plasmon resonance," *Sens. Actuators, B* **11**(1-3), 63–72 (1993).
2. L. Wu, J. Guo, X. Dai, Y. Xiang, and D. Fan, "Sensitivity Enhanced by MoS₂-Graphene Hybrid Structure in Guided-Wave Surface Plasmon Resonance Biosensor," *Plasmonics* **13**(1), 1–7 (2018).
3. Y. Zeng, J. Zhou, X. Wang, X. Wang, and Y. Shao, "Wavelength-scanning surface plasmon resonance microscopy: A novel tool for real time sensing of cell-substrate interactions," *Biosens. Bioelectron.* **145**, 111717 (2019).
4. J. Zhou, Y. Zeng, X. Wang, C. Wu, Z. Cai, G. Bruce, D. Gu, and Y. Shao, "The capture of antibodies by antibody-binding proteins for ABO blood typing using SPR imaging-based sensing technology," *Sens. Actuators, B* **304**, 127391 (2020).
5. Y. Zeng, R. Hu, L. Wang, D. Gu, J. He, S. Y. Wu, H. P. Ho, X. Li, J. Qu, G. Bruce, and Y. Shao, "Recent advances in surface plasmon resonance imaging: detection speed, sensitivity, and portability," *Nanophotonics* **6**(5), 1017–1030 (2017).
6. A. Karabchevsky, S. Karabchevsky, and I. Abdulhalim, "Fast Surface Plasmon Resonance imaging sensor using Radon Transform," *Sens. Actuators, B. Chem.* **155**(1), 361–365 (2011).
7. A. Karabchevsky, S. Karabchevsky, and I. Abdulhalim, "Nano-precision algorithm for Surface Plasmon Resonance determination from images with poor contrast," *J. Nanophotonics* **5**(1), 051813 (2011).
8. X. D. Hoa, A. G. Kirk, and M. Tabrizian, "Towards integrated and sensitive surface plasmon resonance biosensors: A review of recent progress," *Biosens. Bioelectron.* **23**(2), 151–160 (2007).
9. M. Piliarik and J. Homola, "Surface plasmon resonance (SPR) sensors: approaching their limits?" *Opt. Express* **17**(19), 16505–16517 (2009).
10. J. S. Yuk, S. H. Jung, J. W. Jung, D. G. Hong, J. A. Han, Y. M. Kim, and K. S. Ha, "Analysis of protein interactions on protein arrays by a wavelength interrogation-based surface plasmon resonance biosensor," *Proteomics* **4**(11), 3468–3476 (2004).
11. J. S. Yuk, H. S. Kim, J. W. Jung, S. H. Jung, S. J. Lee, W. J. Kim, J. A. Han, Y. M. Kim, and K. S. Ha, "Analysis of protein interactions on protein arrays by a novel spectral surface plasmon resonance imaging," *Biosens. Bioelectron.* **21**(8), 1521–1528 (2006).
12. L. Liu, Y. He, Y. Zhang, S. Ma, H. Ma, and J. Guo, "Parallel scan spectral surface plasmon resonance imaging," *Appl. Opt.* **47**(30), 5616–5621 (2008).
13. O. Soichi, T. Kaoru, and S. Wakida, "Wavelength-scanning surface plasmon resonance imaging," *Appl. Opt.* **44**(17), 3468–3472 (2005).
14. A. Sereda, J. Moreau, M. Canva, and E. Maillart, "High performance multi-spectral interrogation for surface plasmon resonance imaging sensors," *Biosens. Bioelectron.* **54**, 175–180 (2014).
15. K. Chen, Y. Zeng, L. Wang, D. Gu, J. He, S. Y. Wu, H. P. Ho, X. Li, J. Qu, G. Bruce, and Y. Shao, "Fast spectral surface plasmon resonance imaging sensor for real-time high-throughput detection of biomolecular interactions," *J. Biomed. Opt.* **21**(12), 127003 (2016).
16. Y. Zeng, L. Wang, S. Y. Wu, J. He, J. Qu, X. Li, H. P. Ho, D. Gu, G. Bruce, and Y. Shao, "High-throughput imaging surface plasmon resonance biosensing based on an adaptive spectral-dip tracking scheme [J]," *Opt. Express* **24**(25), 28303–283011 (2016).
17. Y. Zeng, L. Wang, S. Y. Wu, J. He, J. Qu, X. Li, H. P. Ho, D. Gu, G. Bruce, and Y. Shao, "Wavelength-Scanning SPR Imaging Sensors Based on an Acousto-Optic Tunable Filter and a White Light Laser," *Sensors* **17**(1), 90–99 (2017).

18. H. Raether, "Surface plasma oscillations and their applications," in *Physics of Thin Films* (Academic Press, 1977), Vol. 9, pp. 145–258.
19. J. Homola, S. S. Yee, and G. Gauglitz, "Surface Plasmon Resonance Sensors: Review," *Sens. Actuators, B* **54**(1-2), 3–15 (1999).
20. W. Knoll, "Interfaces and thin films as seen by bound electromagnetic waves," *Annu. Rev. Phys. Chem.* **49**(1), 569–638 (1998).
21. S. P. Ng, C. M. Wu, S. Y. Wu, and H. P. Ho, "White-light spectral interferometry for surface plasmon resonance sensing applications," *Opt. Express* **19**(5), 4521–4527 (2011).
22. F. Bardin, A. Bellemain, G. Roger, and M. Canva, "Surface plasmon resonance spectro-imaging sensor for biomolecular surface interaction characterization," *Biosens. Bioelectron.* **24**(7), 2100–2105 (2009).
23. S. Scarano, M. Mascini, A. P. Turner, and M. Minunni, "Surface plasmon resonance imaging for affinity-based biosensors," *Biosens. Bioelectron.* **25**(5), 957–966 (2010).